Electronic structures of transition-metal mono-oxides in the self-interaction-corrected local-spin-density approximation

Masao Arai and Takeo Fujiwara
Department of Applied Physics, University of Tokyo, Tokyo 113, Japan
(Received 9 September 1994)

The electronic structures of transition-metal mono-oxides are calculated using the self-interaction-corrected (SIC) local-spin-density approximation (LSDA). The LSDA-SIC has many solutions and various possible solutions are examined. It is shown that the total energies of these solutions are strongly affected by the choice of exchange-correlation energy functionals. Alternatively, if the solutions are chosen so that all orbitals are localized as Wannier functions, the energy gaps are overestimated by 1.5–3 eV. However, in these solutions, the relative positions of occupied transition-metal d bands and oxygen p bands are consistent with the analysis of photoemission spectroscopy by the cluster configuration-interaction theory.

I. INTRODUCTION

The modern electronic structure calculations are based on the local-spin-density approximation (LSDA) to the density-functional theory (DFT).[1–3] Within this approximation, we can obtain the ground state properties from the variational principle for the energy functional $E^{\mathrm{LSDA}}[n_\uparrow, n_\downarrow]$ of spin density $n_\sigma(\mathbf{r})$ ($\sigma = \uparrow, \downarrow$). In this energy functional, the exchange-correlation (XC) energy is not known exactly and is approximated as the integral of the local exchange-correlation energy, which is determined from the XC energy for the uniform electron gas. Since the correlation energy is not known exactly even for the uniform electron gas, many parametrization schemes are proposed.[4,5]

The LSDA has been widely applied to atoms, molecules, and solids.[3] While it has succeeded to explain the ground state properties of a variety of materials, the failures of this approximation are also known. The most serious one is an underestimation of energy gaps for semiconductors and insulators. The suppression of magnetic ordering for antiferromagnetic insulators is also known as a failure of the LSDA. For transition-metal mono-oxide insulators (MnO, CoO, FeO, and NiO), the relative positions of transition-metal d bands and oxygen p bands are inconsistent with the analysis of photoemission spectroscopy by cluster configuration-interaction (CI) theory.[6–10] These relative positions are important to clarify whether they are Mott-Hubbard insulators or charge-transfer insulators. In Mott-Hubbard insulators, the occupied d bands of transition-metal atoms appear at higher energy than the occupied p bands of oxygen atoms, while the relative positions are reversed in charge-transfer insulators. The lowest unoccupied band is, in both cases, transition-metal d states. In the LSDA, the transition-metal d bands appear at higher energy than oxygen p bands[11] and therefore they were considered as Mott-Hubbard-type materials. Such LSDA results do not agree with those by experiments and the CI theory, where MnO is assigned as intermediate of a charge-transfer and Mott-Hubbard insulator and NiO as a charge-transfer insulator.

The purpose of the present paper is to study whether these problems in the LSDA are improved by the self-interaction correction (SIC).[12] The SIC removes unphysical self-interaction for occupied electrons and decreases occupied orbital energies. Perdew and Zunger[12] applied the LSDA SIC to isolated atoms and showed that the highest occupied orbital energies are in better agreement with experimental ionization energies. From these results, the SIC is expected to improve the electronic structures of the insulators and semiconductors.[13–17] However, the application of the LSDA SIC to solids has severe problems since the LSDA SIC energy functional is not invariant under the unitary transformation of the occupied orbitals and we can construct many solutions in the LSDA SIC. If we choose Bloch orbitals, the orbital charge densities vanish in the infinite volume limit. Thus the SIC energy is exactly zero for such orbitals. This does not mean that the SIC is unnecessary for solids since we can construct localized Wannier orbitals that have finite SIC energies. In many calculations for solids, the SIC was adapted to the localized orbitals, which are selected under some physical assumption. These methods have partly succeeded to improve the electronic structures of wide-gap insulators[13] and semiconductors.[14,15]

Recently, Svane and Gunnarsson[16] and Szotek *et al.*[17] performed self-consistent calculations for the transition-metal mono-oxides within the LSDA SIC and obtained the energy gaps and magnetic moments, which are in good agreement with experiments. They did not impose any physical assumption and chose the solutions from a comparison of the total energies. The selected solutions are composed from localized orbitals for transition-metal d bands and extended Bloch orbitals for oxygen p bands. In other words, the SIC is effective only for the transition-metal d orbitals and the oxygen p orbitals are not affected directly by the SIC.

In this paper, we present our results for the transition-metal mono-oxides (MnO, FeO, CoO, and NiO) by the LSDA SIC. We carefully examine the criterion to choose

orbitals. We try both solutions with localized and extended oxygen p orbitals. As an XC energy, both parametrizations proposed by Barth and Hedin[4] (BH) and Vosko *et al.*[5](VWN) are used. We show that the choice of the XC energy functional influences the comparison of the total energies for various solutions.

We also study the relative positions of transition-metal d bands and oxygen p bands to solve the discrepancy between the LSDA and experiments. Previous results by the LSDA SIC (Refs. 16 and 17) predict all materials as charge-transfer insulators and do not agree with the CI theory. We show that the relative positions of occupied bands are consistent with CI theory if the solutions with localized orbitals are chosen.

This paper is organized as follows. In Sec. II we explain the LSDA SIC and our calculation scheme. Special attention is paid to the criterion to choose the orbitals. We show our results for transition-metal mono-oxides in Sec. III and discussions in Sec. IV. Section V is a summary.

II. THEORY

A. LSDA

The LSDA energy functional is defined as

$$E^{\mathrm{LSDA}}[n_\uparrow, n_\downarrow] = T_0[n_\uparrow, n_\downarrow] + \int d^3r V_{\mathrm{ext}}(\mathbf{r}) n(\mathbf{r}) + E_H[n] + E_{\mathrm{XC}}^{\mathrm{LSDA}}[n_\uparrow, n_\downarrow], \quad (2.1)$$

where $n(\mathbf{r}) = n_\uparrow(\mathbf{r}) + n_\downarrow(\mathbf{r})$. The T_0 is the kinetic energy for a noninteracting system with the same spin density $n_\sigma(\mathbf{r})$, V_{ext} is an external potential, E_H is a static Coulomb energy (Hartree energy), and $E_{\mathrm{XC}}^{\mathrm{LSDA}}$ is an exchange-correlation energy within the local-spin-density approximation. From the variation of Eq. (2.1), the Kohn-Sham equation can be obtained as

$$H_{\mathrm{LSDA}}^\sigma \psi_{j\sigma}(\mathbf{r}) = \varepsilon_j^\sigma \psi_{j\sigma}(\mathbf{r}), \quad (2.2)$$

$$H_{\mathrm{LSDA}}^\sigma = -\frac{1}{2m}\Delta + V_{\mathrm{ext}}(\mathbf{r}) + \int \frac{n(\mathbf{r}')}{|\mathbf{r}-\mathbf{r}'|} d^3r' + \frac{\delta E_{\mathrm{XC}}^{\mathrm{LSDA}}[n_\uparrow, n_\downarrow]}{\delta n_\sigma(\mathbf{r})}, \quad (2.3)$$

where the last term is an XC potential $V_{\mathrm{XC}}^\sigma(\mathbf{r})$. Thus we can calculate electronic structures by solving the Kohn-Sham equation self-consistently.

Strictly speaking, the SIC is not directly included in the energy functional defined by Eq. (2.1). The energy functional of orthonormalized one-particle orbitals $\{\psi_{i\sigma}\}$ must be constructed instead of a functional of spin density.[12]

The kinetic energy T_0 in Eq. (2.1) can be written as

$$T_0[n_\uparrow, n_\downarrow] = \min_{\{\psi_{i\sigma}\}} \sum_{i\sigma} \langle \psi_{i\sigma} | -\Delta | \psi_{i\sigma} \rangle, \quad (2.4)$$

where minimization is taken over for all Slater determinants $\{\psi_{i\sigma}\}$ with spin density n_σ. Inserting (2.4) in Eq. (2.1), we can obtain the energy functional for $\{\psi_{i\sigma}\}$,

$$\tilde{E}^{\mathrm{LSDA}}[\{\psi_{i\sigma}\}] = \sum_{i\sigma} \langle \psi_{i\sigma} | -\Delta | \psi_{i\sigma} \rangle + \int d^3r V_{\mathrm{ext}}(\mathbf{r}) n(\mathbf{r}) + E_H[n] + E_{\mathrm{XC}}^{\mathrm{LSDA}}[n_\uparrow, n_\downarrow]. \quad (2.5)$$

It is easily verified that the minimization of Eq. (2.1) with respect to spin density is equivalent to the minimization of Eq. (2.5) to the one-particle orbitals $\{\psi_{i\sigma}\}$. The Kohn-Sham equation (2.2) can be also obtained from the Euler-Lagrange equations for Eq. (2.5). This energy functional is corrected for the self-interaction as explained in the next subsection.

B. LSDA SIC

In the LSDA, the d bands in the transition-metal oxides split by the spin-dependent XC potentials and symmetry of crystals. According to Ref. 11, the NiO and MnO become insulators by these effects. The calculated energy gaps are, however, 1.0 eV (MnO) and 0.4 eV (NiO), which is 10–25% of the experimental values 3.6–3.8 eV for MnO and 4.0–4.3 eV for NiO. For other transition-metal mono-oxides, the spin-dependent exchange-correlation potential and the crystal field splitting in the LSDA are not enough to predict the insulating ground states.

As Mott[18] proposed, the on-site Coulomb repulsion U for the d orbitals on transition metals is important to understand the electronic structures of transition-metal oxides. It splits the one-particle energies for the occupied and unoccupied d orbitals. The LSDA fails to reproduce this splitting. This shortcoming of the LSDA also appears in the calculation of isolated atoms. Namely, the LSDA gives almost the same one-particle energies for the occupied and unoccupied d orbitals with the same spin since both orbitals experience the same local effective potential. On the other hand, they have different energy in the Hartree-Fock (HF) approximation since the effective potentials are nonlocal. Thus, even for the actual transition-metal oxides, we may get larger energy gaps by the HF approximation.

This difference between the LSDA and the HF approximation arises from the treatment of the exchange energy. The HF approximation uses the exact exchange energy and the effective one-body potentials are nonlocal. On the other hand, the exchange energy in the LSDA is approximated by the function of the local spin density and the effective potentials are approximated by the local form. As a result, the self-Coulomb energy $E_H[n_{i\sigma}]$ and self-exchange energy $E_{\mathrm{XC}}^{\mathrm{LSDA}}[n_{i\sigma}]$ for orbital $\psi_{i\sigma}$ with charge density $n_{i\sigma}(\mathbf{r}) = |\psi_{i\sigma}(\mathbf{r})|^2$ do not cancel out and the self-interactions remain finite. This means that occupied electrons experience unphysical potentials by themselves. These unphysical potentials raise the one-particle

energies of occupied orbitals. To overcome this failure, the self-interaction correction[12,19] is formulated by using the energy functional

$$\tilde{E}^{\text{LSDA SIC}}[\{\psi_{i\sigma}\}] = \tilde{E}^{\text{LSDA}}[\{\psi_{i\sigma}\}] + \sum_{i,\sigma} E_{\text{SIC}}[n_{i\sigma}]. \tag{2.6}$$

In this expression, the E_{SIC} is defined as

$$E_{\text{SIC}}[n_{i\sigma}] = -\left\{E_H[n_{i\sigma}] + E_{\text{XC}}^{\text{LSDA}}[n_{i\sigma}, 0]\right\} \tag{2.7}$$

and removes the self-interaction explicitly. The variational procedure of Eq. (2.6) with respect to $\psi_{i\sigma}$ yields

$$\{H_{\text{LSDA}}^{\sigma} + V_{\text{SIC}}^{i\sigma}(\mathbf{r})\}\psi_{i\sigma}(\mathbf{r}) = \sum_j \psi_{j\sigma}(\mathbf{r})\varepsilon_{ji}^{\sigma}, \tag{2.8}$$

$$V_{\text{SIC}}^{i\sigma}(r) = -\left\{\int \frac{n_{i\sigma}(r')}{|r-r'|}d^3r' + \frac{\delta E_{\text{XC}}^{\text{LSDA}}[n_{i\sigma}, 0]}{\delta n_{i\sigma}(r)}\right\}. \tag{2.9}$$

The $V_{\text{SIC}}^{i\sigma}$ is a SIC potential for an orbital $\psi_{i\sigma}$ and removes the unphysical self-interaction potential. The Lagrange multipliers ε_{ji}, which are introduced to ensure the orthogonality of $\{\psi_{i\sigma}\}$, must satisfy the localization condition $\varepsilon_{ji}^{\sigma} = (\varepsilon_{ij}^{\sigma})^*$ so that the total energy is stationary about the unitary transformation of $\psi_{i\sigma}$.[19] From Eq. (2.8) $\varepsilon_{ij}^{\sigma}$ satisfies

$$\begin{aligned}\varepsilon_{ij}^{\sigma} &= \langle\psi_{i\sigma}|\{H_{\text{LSDA}}^{\sigma} + V_{\text{SIC}}^{i,\sigma}\}|\psi_{j\sigma}\rangle \\ &= \langle\psi_{i\sigma}|\{H_{\text{LSDA}}^{\sigma} + V_{\text{SIC}}^{j,\sigma}\}|\psi_{j\sigma}\rangle.\end{aligned} \tag{2.10}$$

Thus $\varepsilon_{ij}^{\sigma}$ may be considered as a matrix element of an effective one-body Hamiltonian. One-particle energies for occupied orbitals are obtained by diagonalizing the Lagrange multiplier matrix. (One-particle states that diagonalize $\varepsilon_{ij}^{\sigma}$ are called canonical orbitals.[19]) For unoccupied states, we diagonalize the LSDA Hamiltonian in the subspace orthogonal to the occupied orbitals.

To end this section, we comment about the relation between the SIC and the DFT. Since the energy defined by Eq. (2.6) is a functional of orbitals, it is not directly connected to the DFT. We can define the energy functional of spin density by constrained minimization as

$$E^{\text{LSDA SIC}}[n_\uparrow, n_\downarrow] = \min_{\{\psi_{i\sigma}\}} \tilde{E}^{\text{LSDA SIC}}[\psi_{i\sigma}]. \tag{2.11}$$

If we use this energy functional, the LSDA SIC can be considered as a DFT where XC energy functional is approximated as

$$\begin{aligned}E_{\text{XC}}^{\text{LSDA SIC}}[n_\uparrow, n_\downarrow] = E_{\text{XC}}^{\text{LSDA}}[n_\uparrow, n_\downarrow] \\ + \left\{\min_{\{\psi_{i\sigma}\}}\left[\sum_{i\sigma}(\langle\psi_{i\sigma}| - \Delta|\psi_{i\sigma}\rangle\right.\right. \\ \left. - E_H[n_{i\sigma}] - E_{\text{XC}}^{\text{LSDA}}[n_{i\sigma}, 0])\right] \\ \left. - T_0[n_\uparrow, n_\downarrow]\right\}.\end{aligned} \tag{2.12}$$

This is a nonlocal self-interaction free XC energy functional. If we derive the Kohn-Sham equations using the above XC energy, the eigenvalues do not agree with those from Eq. (2.8) in general. Thus the one-particle energies calculated in the LSDA SIC do not have a direct relation with the Kohn-Sham eigenvalues. The improvement of orbital energies of isolated atoms by the SIC is attributed to the orbital-dependent potentials which correctly describe the asymptotic behavior and reduce the relaxation effect.[12,20]

C. Choice of orbitals in the LSDA SIC

As mentioned in Sec. I, the energy functional defined by Eq. (2.6) is not invariant under unitary transformation for the occupied orbitals. Therefore the results depend on the choice of orbitals. If we solve the LSDA SIC equations with extended Bloch orbitals, the SIC's do not contribute because the orbital charge densities vanish as (volume)$^{-1}$ in the infinite volume limit. On the other hand, there exist solutions which are assembled from localized Wannier functions. Though these orbitals are not the eigenstate of crystal momentum $\mathbf{k}$, the Lagrange multiplier matrix $\varepsilon_{ij}^{\sigma}$ has translational symmetry. By diagonalizing $\varepsilon_{ij}^{\sigma}$, we recover the energy bands $\varepsilon_{n\mathbf{k}}^{\sigma}$. Since each occupied orbital experiences the attractive SIC potential, the one-particle energies for occupied bands are lowered and rearranged. These results are completely different from those by the LSDA. Thus, to apply the LSDA SIC to solids, we need well-defined criteria for a choice of orbitals. Such criteria are especially important if there are many inequivalent orbitals in a unit cell, since each orbital can be chosen as an extended Bloch or a localized Wannier function and we have many solutions in the LSDA SIC.

The most plausible criterion seems to be the choice of the lowest energy solution[16,17] since the LSDA is based on the variational principle. Another criterion is that of the localized orbitals[13,15,14] because the LSDA SIC has been successfully applied to atoms[12] and molecules.[19] Until recently, these two criteria were believed to be equivalent, i.e., the localized orbitals were believed to give the lowest energy. While this would be true for wide-gap insulators, the lowest energy solutions that Svane and Gunnarsson[16] chose for transition-metal oxides are composed from localized transition-metal d orbitals and extended oxygen p orbitals. We discuss the inadequacy of this choice of orbitals and argue that the total energy criterion for the LSDA SIC has a few fundamental problems.

First, the localized orbitals must have the negative SIC energies to become the lowest energy solutions since the SIC energies for the extended orbitals are exactly zero. To investigate this point, we plot the SIC energy for the $1s$-like orbital $\psi(r) = Ce^{-r/A}$ in Fig. 1(a) using various XC energy functionals. If we ignore correlation energy, the SIC energy of this orbital is always negative, as suggested for general orbitals by Perdew and Zunger.[12] The correlation energy, which is smaller than the exchange energy, is responsible for the sign of the SIC energy. As shown in Fig. 1(a), a small difference between the BH

and the VWN XC energy can change the sign of SIC energies. Thus it depends on the XC energy functionals whether the localized orbitals become lowest energy or not.[21] The contribution of the SIC potentials to one-particle energies is plotted in Fig. 1(b). According to this figure, the SIC potentials are attractive in the wide parameter region. Even if the SIC energies are positive, the SIC potentials are attractive. We also find that the form of the XC energy functionals is not important for the SIC potentials compared with their absolute values. These two figures present the different behaviors of the SIC energy and the SIC potential and suggest that the SIC potentials for localized orbitals are important even if the corresponding SIC energies are positive. In other words, the criterion that uses the total energy might be problematic.

Second, the charge densities for extended orbitals vanish only in the infinite volume limits. They remain finite for finite size clusters. If the size of the clusters is fairly small, extended orbitals are energetically unfavorable and the localized orbitals have lowest energy. As the cluster size increases, the SIC energies for extended orbitals become small. Then the lowest energy solutions would change from localized orbitals to extended orbitals if the SIC energies for localized orbitals are positive.[22–24] Therefore, if the lowest energy solution is chosen, the electronic structure would change discontinuously when the cluster size changes. It is unlikely that this discontinuous change has a physical origin since the distinction between the extended and localized orbitals is introduced by the SIC and does not exist in the HF approximation or the LSDA. On the other hand, if we apply the SIC to localized orbitals and choose the lowest energy solutions within such orbitals, we can get solutions where all orbitals are affected by the SIC potentials. These solutions are directly related to corresponding atomic or cluster calculations and do not have any discontinuous changes as cluster size increases. Thus the SIC for localized orbitals is a natural extension to the SIC for atoms or small clusters.

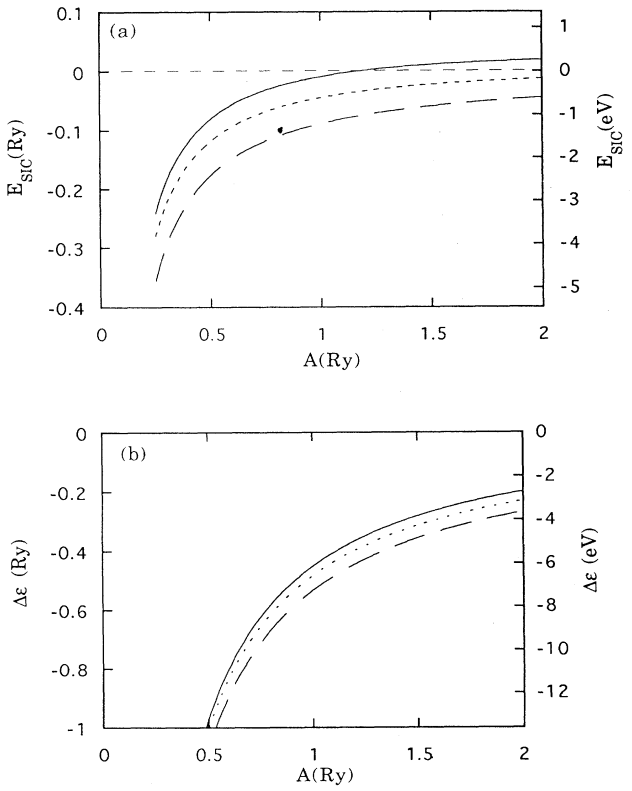

FIG. 1. (a) The SIC energy and (b) the contribution of the SIC potential to one-particle eigenvalue ($\Delta\varepsilon = \langle\psi|V_{\rm SIC}|\psi\rangle$) as a function of A for the $1s$-like orbital $\psi(r) = Ce^{-r/A}$. Solid lines represent the results by the BH and dotted lines by the VWN. The dashed lines are the results for which the correlation energy is ignored.

D. Adoption of the SIC in the linear muffin-tin-orbital method

To calculate charge densities of localized orbitals, the basis sets of extended wave functions such as plain waves are not appropriate. The localized basis set is necessary. We use the linear muffin-tin-orbital[25] (LMTO) method with the atomic sphere approximation. The notation in this paper is the same as in Ref. 25.

The basis functions of the LMTO are written as

$$|\chi_{RL}\rangle = |\phi_{RL}\rangle + \sum_{R',L'} |\dot{\phi}_{R'L'}\rangle h_{R'L',RL}, \qquad (2.13)$$

where R and L denote atomic sites and angular momenta (l, m), respectively. The spin index σ is omitted for simplicity. ϕ_{RL} is a solution of the Schrödinger equation with fixed energy E_ν in each atomic sphere and $\dot{\phi}_{RL}$ is its energy derivative. They are created by solving the radial Schrödinger equations without SIC potentials. Due to the second term in Eq. (2.13), the $|\chi_{RL}\rangle$ has a tail within a region of a few neighbor atoms around the central atom at R and slightly overlapped with each other. In the LSDA, we may ignore these overlaps and treat them by first-order perturbation theory.[25] However, in the present calculation, these overlaps are important because the spatial extents of orthogonal orbitals determine the SIC energies and potentials. If we ignore the overlaps between LMTO basis functions, the orbitals ψ_i can be more localized and the absolute values of the SIC energies would be overestimated. We therefore treat the overlaps rigorously.

The localized orbitals ψ_i are described by the linear combination of $|\chi_{RL}\rangle$,

$$|\psi_i\rangle = \sum_{R,L} |\chi_{RL}\rangle U_{RL,i}. \qquad (2.14)$$

The energy functional in Eq. (2.6) is evaluated for these orbitals. To solve Eq. (2.8), we use simulated annealing methods,[23]

$$\frac{d}{dt}|\psi_i\rangle = -\gamma \left\{ [H_{\rm LSDA} + V^i_{\rm SIC}]\,|\psi_i\rangle - \sum_j |\psi_j\rangle \varepsilon_{ji} \right\}. \tag{2.15}$$

Equation (2.15) is integrated numerically using the discrete time slice Δt. The Lagrange multipliers ε_{ji} are chosen as

$$\varepsilon_{ij} = \frac{1}{2}\{\langle\psi_i|\{H_{\rm LSDA} + V^i_{\rm SIC}\}|\psi_j\rangle + \langle\psi_i|\{H_{\rm LSDA} + V^j_{\rm SIC}\}|\psi_j\rangle\}\ , \tag{2.16}$$

so that the orthogonality condition to $\{\psi_i\}$ holds during the time evolution. When $\frac{d}{dt}|\psi_i\rangle = 0$ is achieved, the orbitals satisfy the LSDA SIC equations and the localization condition $\varepsilon_{ji} = (\varepsilon_{ij})^*$. From Eqs. (2.14) and (2.15) we get

$$\frac{d}{dt}U_{RL,i} = -\gamma\Big\{ \sum_{R',L'} (\mathbf{O^{-1}H})_{RL,R'L'} U_{R'L',i} + \sum_{R',L'} \mathbf{O^{-1}}_{RL,R'L'} \langle\chi_{R'L'}|V^i_{\rm SIC}|\psi_i\rangle - \sum_j U_{RL,j}\varepsilon_{ji}\Big\}, \tag{2.17}$$

where

$$\mathbf{H}_{RL,R'L'} = \langle\chi_{RL}|H_{\rm LSDA}|\chi_{R'L'}\rangle, \tag{2.18}$$

$$\mathbf{O}_{RL,R'L'} = \langle\chi_{RL}|\chi_{R'L'}\rangle. \tag{2.19}$$

The term $\mathbf{O}^{-1}$ in Eq. (2.17) makes the calculation in real space difficult. We assume translational symmetry with periodically aligned localized orbitals. Under this assumption, the orbital index j can be written as $(n, \mathbf{T})$, where n denotes orbitals in a unit cell and $\mathbf{T}$ is a translational vector. By this symmetry, we can transform Eq. (2.17) into reciprocal space

$$\frac{d}{dt}U^{\mathbf{k}}_{rL,n} = -\gamma\Big\{ \sum_{r'L'} (\mathbf{O^{-1}H})^{\mathbf{k}}_{rL,r'L'} U^{\mathbf{k}}_{r'L',n} + \sum_{r',L'} \mathbf{O^{-1}}^{\mathbf{k}}_{rL,r'L'} V^{\mathbf{k}}_{r'L',n} - \sum_m U^{\mathbf{k}}_{rL,m}\varepsilon^{\mathbf{k}}_{mn}\Big\}, \tag{2.20}$$

$$V^{\mathbf{k}}_{rL,n} = \sum_{\mathbf{T}} e^{-i\mathbf{k}\cdot\mathbf{T}} \langle\chi_{r'L'}|V^n_{\rm SIC}|\psi_n\rangle, \tag{2.21}$$

$$U^{\mathbf{k}}_{rL,n} = \sum_{\mathbf{T}} e^{-i\mathbf{k}\cdot\mathbf{T}} U_{(r,\mathbf{T})L,n}, \tag{2.22}$$

where r denotes atomic sites in a unit cell and $(r, \mathbf{T})$ is a composite label for atomic sites. Since the size of matrix in Eq. (2.20) is determined by the number of atoms in a unit cell, it is easily calculated as in the standard band theory.

The $\langle\chi_{rL}|V^n_{\rm SIC}|\psi_n\rangle$ must be calculated in real space. We use a supercell and corresponding k points to calculate $U_{RL,j}$ and $U^{\mathbf{k}}_{rL,n}$. In the following, the supercell with 500 atoms was used. The orbital charge densities and the SIC potentials are expanded to the linear combination of the spherical harmonics in each atomic sphere. About 50 atoms around the central atom are treated. This approximation can be justified since the self-consistent orbitals are localized within a few neighbor atoms. Details of the calculation are presented in the Appendix.

In our program code, the calculation of the nonspherical XC energy and the potential consumes much CPU time because of the nonlinearity of the XC energy functional. Therefore, most calculations were performed under the spherical approximation to the orbital charge densities. The contribution of the nonspherical SIC will be discussed in Sec. IV.

III. RESULTS

We calculated the electronic structures of TO (T=Mn, Fe, Co, and Ni). Below Néel temperature, they are antiferromagnetic insulators. Magnetic moments on the transition-metal atoms in a [111] plane are aligned in the same direction and they are in opposite directions in successive planes. We use perfect rock-salt structures with lattice constants listed in Table I. In the ionic description, these materials are understood as $T^{2+}O^{2-}$ with $[\mathrm{Ar}]3d^n4s^0$ configuration for the transition-metal and $[1s^22s^2]2p^6$ for the oxygen. The Ar-shell of transition-metal ions and the 1s shell of oxygen ions are treated as frozen cores. The oxygen $2s$ bands appear about 0.7–1.0 Ry below other valence bands and have small dispersions. They are self-consistently determined in the LSDA using a different energy panel from other valence bands and are fixed to this self-consistent charge density in the LSDA SIC calculations. Thus the valence bands are generated from the transition-metal d level and the oxygen p level. The initial wave functions are chosen to satisfy these configurations, i.e., they have n localized d orbitals on a transition-metal atom and six on an oxygen atom. The occupied orbitals on the transition-metal atoms are chosen so as to maximize spin magnetic moments. Since each orbital extends to neighbor atoms, the actual ionicity in each atomic sphere need not be ± 2 and depends on the size of atomic sphere radii. We choose them as presented in Table I so that each sphere maintains almost charge neutrality in the LSDA.

We choose three kinds of possible solutions. In the type 1 solution all orbitals are extended. For this solution,

TABLE I. The lattice constants, average atomic sphere radii ($S_{\rm av}$), and atomic sphere radii used in the present calculations (S_T for transition metal, $S_{\rm O}$ for oxygen).

Parameter (a.u.)	MnO	FeO	CoO	NiO
Lattice constant[a]	8.381	8.145	8.050	7.927
$S_{\rm av}$	2.600	2.526	2.497	2.488
S_T	2.993	2.884	2.832	2.749
$S_{\rm O}$	2.027	2.020	2.035	2.077

[a]Reference 30.

the results are the same as those by the LSDA. In the type 2 solution all orbitals are localized. In the type 3 solution transition-metal d orbitals are localized and oxygen p orbitals are extended. These three types of solutions exist at least as stationary points for the LSDA SIC energy functional.

We found that the physical properties such as energy gaps or magnetic moments are not sensitive in each case to the choice of the XC energy functional. In the following, we present the results by the BH XC energy functional. Only the comparison of the total energies depends on the choice of the XC energy functional, which will be discussed in Sec. IV.

A. Type 1 (LSDA)

To compare with other solutions, we briefly summarize the results for type 1 (LSDA). The calculated energy bands are shown in Fig. 2. Narrow d bands appear at higher energy than the oxygen p bands for all compounds. By the spin-dependent XC potential, the d bands split into five majority and minority spin bands. For MnO, the energy gap appears between them. The five bands also split into two e_g bands and three t_{1g} bands by the symmetry of crystals. While NiO has a small energy gap between them in the previous calculation,[11] the present one does not give an energy gap and e_g and t_{1g} bands slightly overlap. The origin of this discrepancy is attributed to the difference of atomic sphere radii and the treatment of oxygen $2s$ orbitals. If we choose the same atomic sphere radii for both Ni and O and treat the oxygen $2s$ bands in the same energy panel with other valence bands, we get the an energy gap of 0.4 eV. From this observation, we should point out that the relative positions of the energy bands shift < 0.5 eV by these different approximations. The energy gaps and magnetic moments are listed in Table II. The energy gap for MnO is 1.1 eV, which is about 30% of experimental value 3.6–3.8 eV. For other compounds, there are no energy gaps. The magnetic moments are also underestimated in the LSD. Especially for NiO, the agreement with experiments is worse.

B. Type 2

The calculations were performed from the initial wave functions in which each orbital is completely localized on one LMTO basis function. When the convergence is achieved, each orbital is extended to neighboring atoms. For MnO, 94% of the orbital charge density of a transition-metal d orbital stays inside the central atoms and 75% of that for an oxygen p orbital. This result indicates that the transition-metal d orbitals are more localized than the oxygen p orbitals.

The energy bands are shown in Fig. 3. The attractive SIC potentials shift the occupied bands downward and we get larger energy gaps for all compounds. These changes are not the simple rigid shifts since the SIC potentials depend on the spatial extents of orbitals. The transition-metal d orbitals are more localized than oxygen p orbitals. Thus the SIC potentials are larger in d orbitals. As a result, the d bands and p bands, which exist separately in the LSDA, appear at the same energy region and strongly hybridize. The unoccupied bands slightly shift upward by 0–1 eV and the lowest band has weights mainly on transition-metal d orbitals.

We list the magnetic moments and energy gaps in Table II. The energy gaps are 1.5–3 eV larger than experimental values. The magnetic moments also increase by the SIC and agree with experiments for MnO and NiO. For FeO and CoO, they do not agree with experiments. It is probably due to the neglect of the spin-orbit interaction and orbital polarization.[16,17]

The main difference between these compounds appears in the partial density of states (PDOS) as shown in Fig. 4. For MnO, the PDOS for oxygen and a transition metal distribute in the whole region of occupied bands. While the distribution of oxygen PDOS is uniform, the distri-

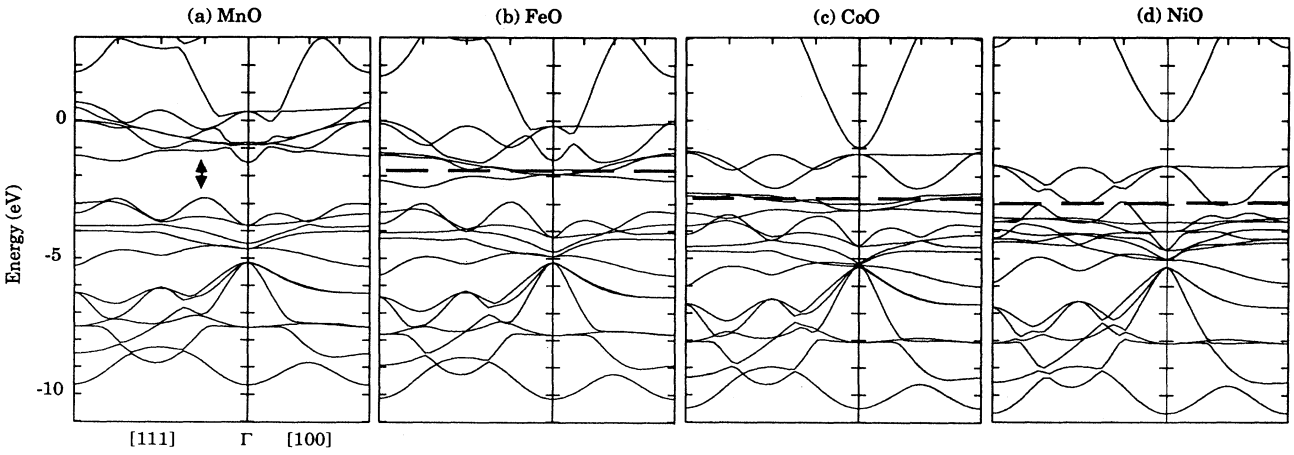

FIG. 2. The energy bands by type 1 (LSDA) in the [111] and [100] directions. The dashed lines represent Fermi energies and the arrow indicates the energy gap.

TABLE II. Band gaps and magnetic moments.

	Band gap (eV)				Spin magnetic moment (μ_B)			
Compound	Type 1 (LSD)	Type 2	Type 3	Expt.[a]	Type 1 (LSD)	Type 2	Type 3	Expt.[a]
MnO	1.1	6.5	3.4	3.6–3.8	4.5	4.7	4.7	4.79,4.58
FeO	0.0	6.1	3.4		3.2	3.7	3.6	3.32
CoO	0.0	5.3	2.7	2.4	2.0	2.7	2.6	3.35,3.38
NiO	0.0	5.6	2.8	4.0,4.3	0.7	1.7	1.5	1.77,1.64,1.93

[a]Reference 16.

butions of transition-metal PDOS has peaks at a lower energy region. This indicates that the Mn d orbitals have slightly lower energy than oxygen p orbitals. For NiO, the Ni PDOS shifts to lower energy and they have sharp peaks. Therefore, the separation of the d level and the p level is larger for NiO than for MnO.

To compare the relative energy of d orbitals and p orbitals, we list the average values of diagonal elements of Lagrange multipliers $\varepsilon_{ij}^{\sigma}$ in Table III. These values are one-particle energies when all hybridizations are switched off. The energy difference $\langle\varepsilon_d\rangle - \langle\varepsilon_p\rangle$ is 1.3 eV for MnO and 2.9 eV for NiO, where $\langle\varepsilon_d\rangle$ and $\langle\varepsilon_p\rangle$ are average values of occupied transition-metal d orbitals and oxygen p orbitals, respectively. We compare these values with the difference between the charge-transfer gap Δ and the Coulomb energy U obtained from the analysis of photoemission spectroscopy by CI theory.[8] These values can be a measure of the difference of orbital energies between the transition-metal d level and the oxygen p level. The $U - \Delta$ for MnO and FeO are 0.5 eV and 0.8 eV, respectively. They are about 3 eV smaller than that for NiO. We found that such a qualitative difference between these materials is reproduced by the $\langle\varepsilon_d\rangle - \langle\varepsilon_p\rangle$, though they are slightly larger than $U - \Delta$ for MnO and FeO and smaller for NiO. If we take into account the different definitions of $\langle\varepsilon_d\rangle - \langle\varepsilon_p\rangle$ and $U - \Delta$, we can conclude that the relative positions of d bands and p bands are consistent with the CI theory.

C. Type 3

The energy bands and PDOS for type 3 solutions are shown in Figs. 5 and 6. In these solutions, oxygen p orbitals are Bloch functions and are not influenced by the SIC potentials directly. They are indirectly affected by the SIC potentials for transition-metal d orbitals through orthogonalization of orbitals and charge redistribution. Thus the positions of oxygen p bands are almost unchanged while the transition-metal d bands shift about 10 eV and appear below oxygen p bands. As a result, the relative positions of d bands and p bands are reversed from the LSDA for all compounds. The highest occupied level has weights mainly on oxygen p orbitals and slightly mixed with transition-metal d orbitals. Therefore, all compounds are described as charge-transfer-type insulators.

The diagonal elements of Lagrange multipliers are pre-

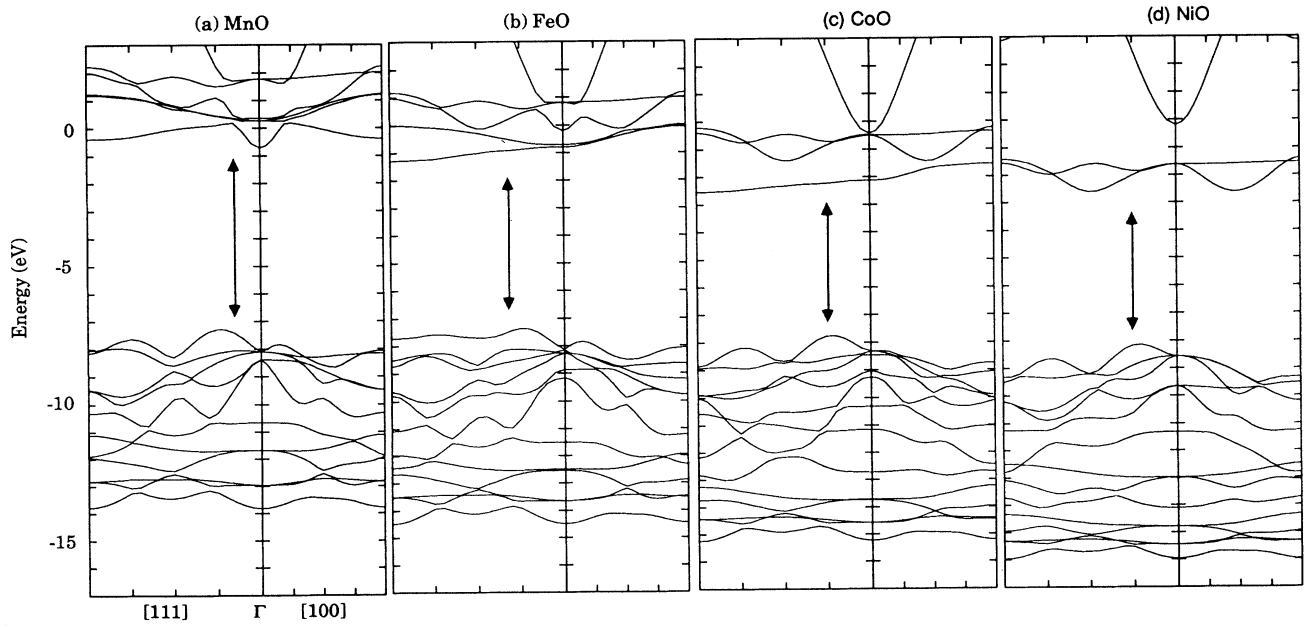

FIG. 3. The energy bands by type 2 in the [111] and [100] directions. The arrows indicate the energy gaps.

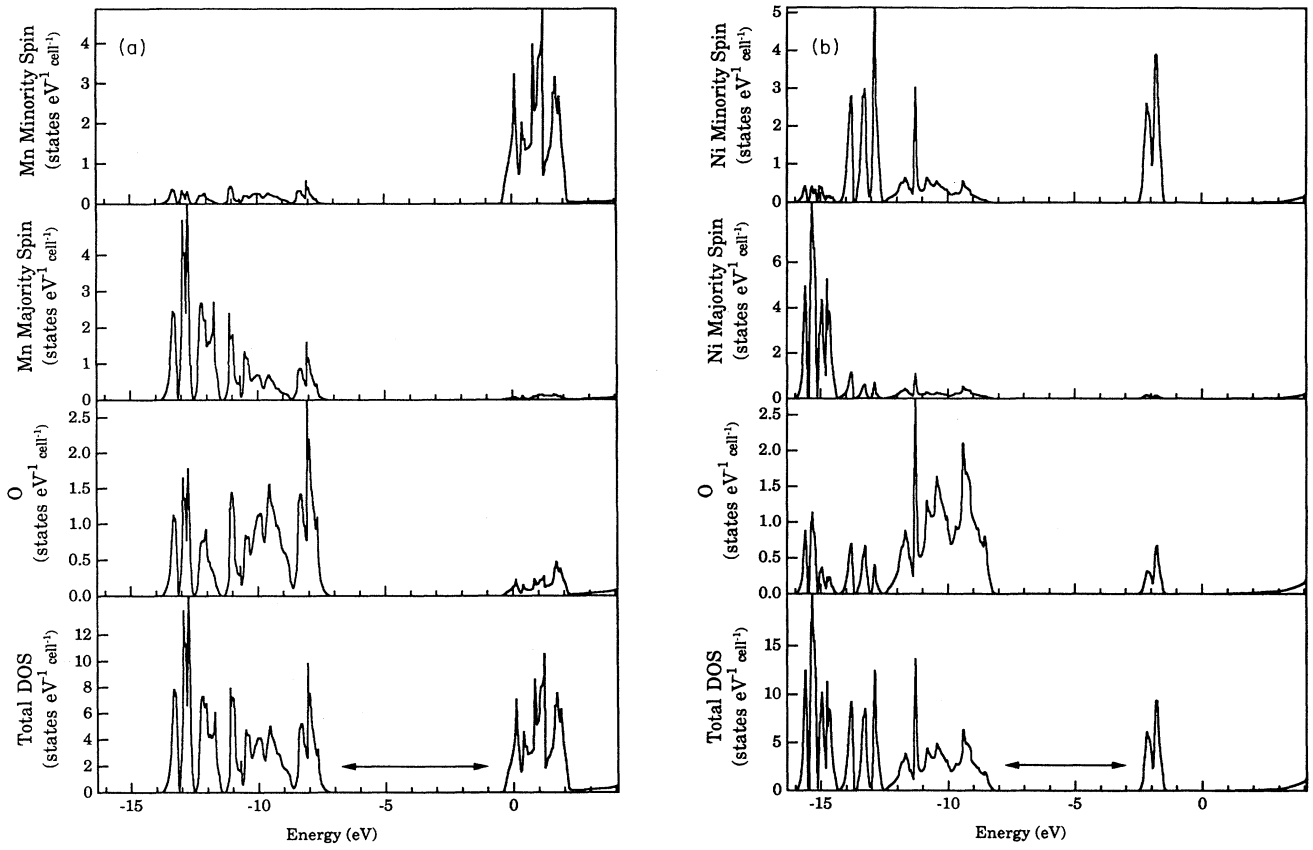

FIG. 4. Total and partial density of states of (a) MnO and (b) NiO for type 2. The arrows indicate the energy gaps.

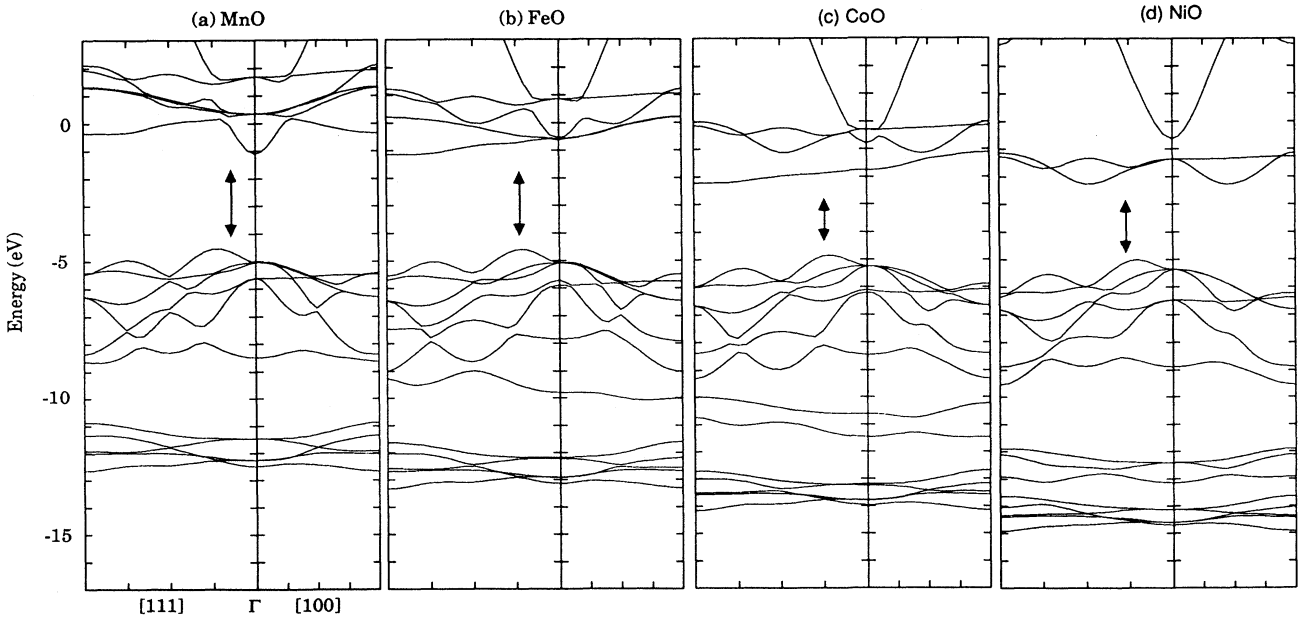

FIG. 5. The energy bands by type 3 in the [111] and [100] directions. The arrows indicate the energy gaps.

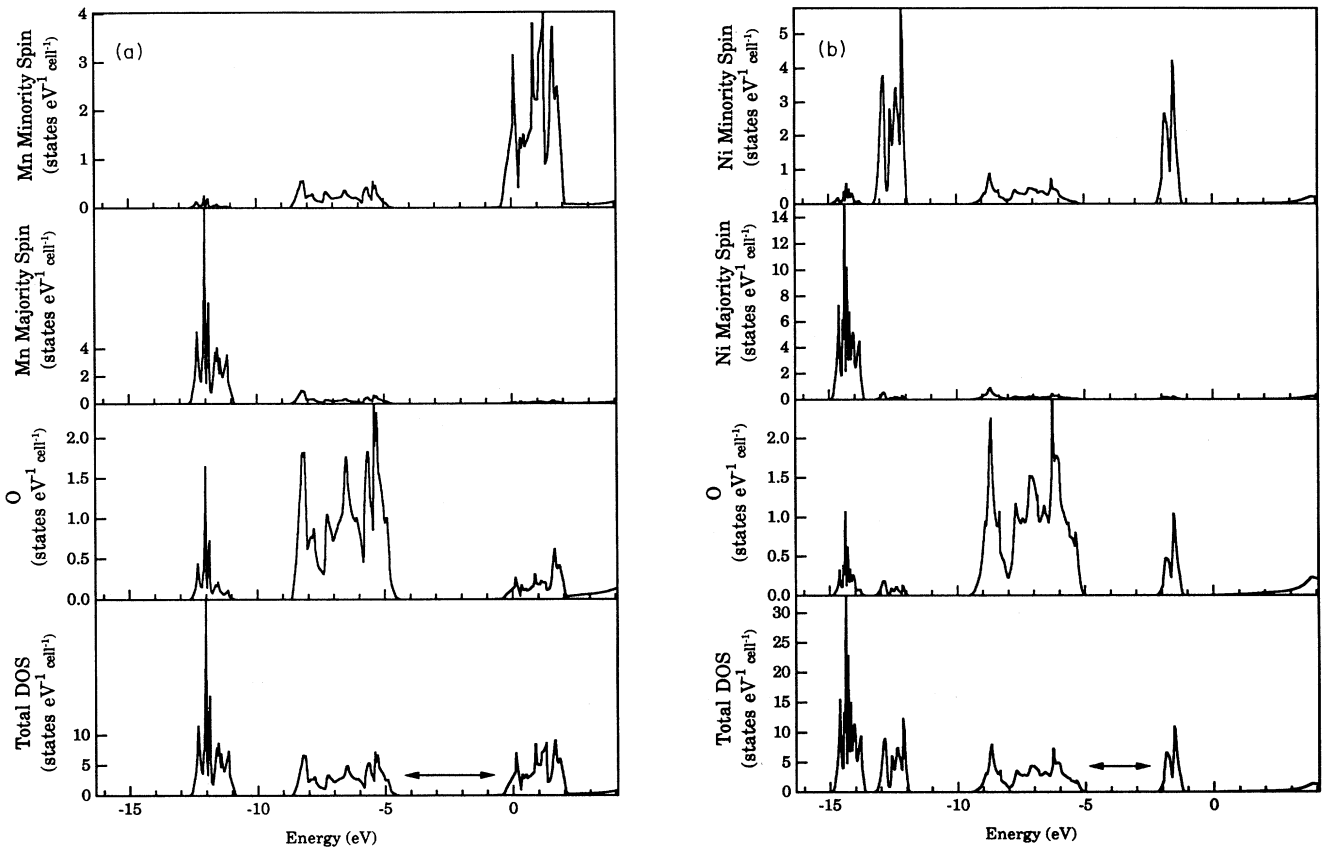

FIG. 6. Total and partial density of states of (a) MnO and (b) NiO for type 3. The arrows indicate the energy gaps.

sented in Table III. The energy differences $\langle \varepsilon_p \rangle - \langle \varepsilon_d \rangle$ are 4.2–5.7 eV, which also indicates that all compounds are described as charge-transfer insulators. Thus these solutions cannot reproduce the difference between MnO and NiO.

The energy gaps are about 3 eV for all compounds. For MnO and CoO, they are in better agreement with experimental values than those by type 2. For NiO, the energy gap by type 3 is 1–1.5 eV smaller than experiments and the one by type 2 is 1–1.5 eV larger. The magnetic moments are almost the same values as those by type 2. These solutions are chosen by previous works[16,17] from total energy comparison. If we choose these solutions, the results agree with those in Refs. 16 and 17.

IV. DISCUSSION

In Sec. II B, we showed that the total energy criterion has a few problems from a general point of view. Here we compare the total energies of NiO and show that they really depend on the choice of the XC energy functional.

The total energies of NiO with various approximations are presented in Table IV. If the BH is used as the XC energy and the SIC energy is spherically approximated, the type 3 solution has the lowest energy. The energy difference is, however, about 0.3 eV per electron, which is the same magnitude as the difference between the BH and VWN XC functionals. Therefore, the lowest energy solution depends on the choice of the XC energy functional.

TABLE III. Average values of diagonal Lagrange multipliers: $\langle \varepsilon_d \rangle$ for occupied d orbitals and $\langle \varepsilon_p \rangle$ for occupied p orbitals. $U - \Delta$ is the difference between the charge transfer gap Δ and the Coulomb energy U obtained from the analysis of photoemission spectroscopy in Ref. 8 (eV).

	$\langle \varepsilon_d \rangle$		$\langle \varepsilon_p \rangle$		$\langle \varepsilon_p \rangle - \langle \varepsilon_d \rangle$		$U - \Delta$
Compound	Type 2	Type 3	Type 2	Type 3	Type 2	Type 3	
MnO	−11.5	−11.3	−10.3	−6.1	1.3	5.3	0.5
FeO	−11.7	−11.4	−10.6	−7.2	1.2	4.2	0.8
CoO	−12.9	−12.3	−10.8	−7.4	2.1	4.8	
NiO	−13.9	−13.3	−11.0	−7.6	2.9	5.7	3.5

TABLE IV. Total energy (eV/electron) for NiO with various approximations. Nonspherical SIC up to l_{SIC} is included.

XC	l_{SIC}	$E_{type\ 2} - E_{LSDA}$	$E_{type\ 3} - E_{LSDA}$	Lowest energy
BH	0	−0.03	−0.28	type 3
VWN	0	−0.51	−0.57	type 3
BH	4	0.44	0.30	type 1
VWN	4	−0.06	−0.02	type 2

For example, if we use VWN and include the contribution from nonspherical SIC, the lowest energy solution is type 2. As explained in Sec. II B, this dependence on the XC energy arises from the fact that the SIC energies for the extended orbitals are exactly zero, while the ones for localized orbitals depend on the choice of the XC energy. Thus the absolute value of the XC energy is important to compare the total energies within three types of solutions. It is in contrast to the LSDA, where the total energy comparison often cancels the absolute error in the XC energy and the relative energies are insensitive to the choice of the XC energy functional.

As an alternative criterion to the total energy, let us consider choosing the solutions with localized orbitals. In the present calculations, type 2 solutions are chosen for all compounds. As explained in Sec. III B, the description of the occupied bands is consistent with photoemission study. However, they overestimate the energy gaps as opposed to type 3 solutions. In this sense, the SIC for localized orbitals may be similar to the HF approximation.

One possible origin of the overestimation of energy gaps is the treatment of unoccupied orbitals. In the present approximation, the unoccupied bands are not affected directly by the SIC. If the unoccupied orbitals are extended, these approximations may be justified. However, if the excitations observed in experiments have localized character, the present treatment may overestimate their excitation energies. Another possible origin is the failure of the one-body approximation. According to the CI theory, the highest occupied states are generated from many-body effect. The present methods are just a one-body approximation and may fail to reproduce such excitations.

We also applied the LSDA SIC to VO (Fig. 7). Even though the VO is metal, we obtained insulating solutions

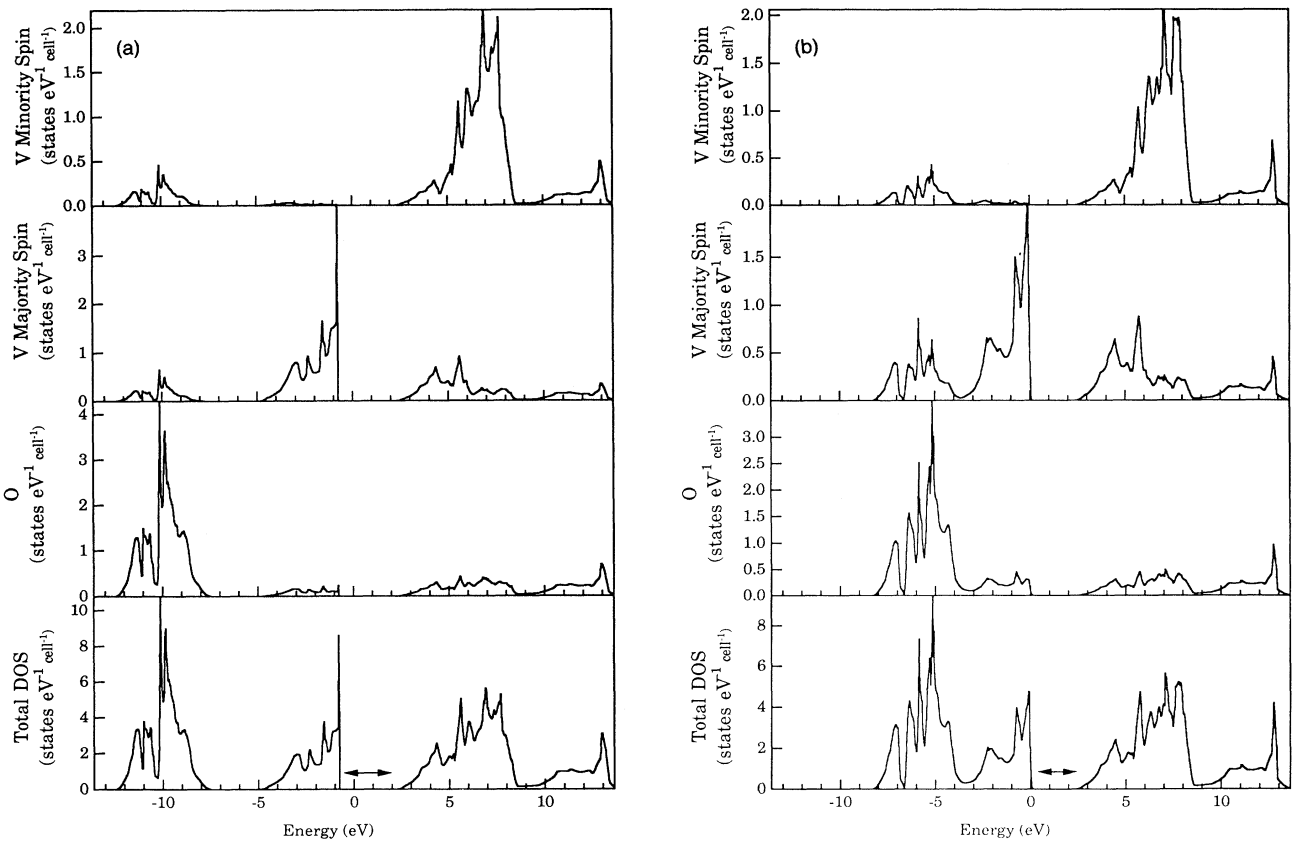

FIG. 7. Total and partial density of states of VO for (a) type 2 and (b) type 3. The arrows indicate the energy gaps.

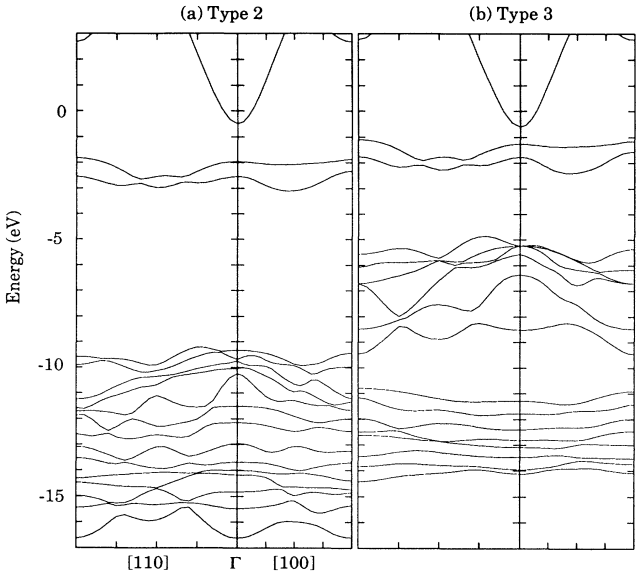

FIG. 8. The energy bands of NiO for (a) type 2 and (b) type 3. The nonspherical contribution of the SIC potentials are included.

for types 2 and 3. Therefore, the criterion to choose the localized orbitals predicts VO as an insulator. This is another problem of the present method. However, we can see the difference between VO and other compounds even in these calculations. The relative positions of energy bands are reversed from other compounds. Namely, the occupied transition-metal d bands appear at higher energy than the oxygen p bands. Thus the VO can be characterized as a Mott-Hubbard-type material.

The advantage of the criterion to choose localized orbitals is that it can be widely applicable for insulators and semiconductors. We are calculating the electronic structures of the semiconductors by the LSDA SIC and these results will be published elsewhere. If the total energy criterion is used for Si, on the other hand, the extended orbitals have lowest energy and the SIC does not contribute.[26] This is in contrast to the improvements of electronic structures by the simplified SIC.[14,15]

Finally, the nonspherical contribution of the SIC to physical properties was examined for NiO. Figure 8 shows the energy bands with nonspherical SIC up to $l \leq 4$. The nonspherical contribution to each orbital does not have the symmetry of crystals. As a consequence, the energy bands split. The relative positions and energy gaps also change at most by 0.5 eV. The overall structure is qualitatively unchanged and the spherically averaged SIC's may be acceptable approximations for physical properties.

V. CONCLUSION

In conclusion, we calculated the electronic structures of transition-metal mono-oxides by the LSDA SIC. Solutions with localized and extended oxygen p orbitals were examined. Both solutions give larger energy gaps and magnetic moments than the LSDA results. From general arguments, we proposed a simple guiding principle that the SIC should be included in all occupied bands of insulators. Such solutions seem to describe occupied states in better agreement with experiments and the CI theory, though they give energy gaps 1.5–3 eV larger than the experimental values. These calculations provide good starting points for further analysis by the GW approximations[27–29] or other methods that incorporate the correlation effect.

ACKNOWLEDGMENTS

This work was supported by a Grant-in-Aid for Scientific Research on Priority Areas from the Ministry of Education, Science, and Culture, Japan. Some of the numerical calculations were performed at the Computer Center of the Institute of Molecular Science.

APPENDIX: EVALUATION OF THE SIC

The charge density of the orbital in Eq. (2.14) can be written as

$$n(\mathbf{r}) = \sum_{R,L} \theta_R(\mathbf{r}) \frac{1}{\sqrt{4\pi}} n_{RL}(r) Y_L(\hat{r}), \tag{A1}$$

$$n_{RL}(r) = \sqrt{4\pi} \sum_{L_1,L_2} C_{LL_1L_2} [U^*_{RL_2} U_{RL_3} \phi^*_{Rl_2}(r)\phi_{Rl_3}(r) + \tilde{U}^*_{RL_2} U_{RL_3} \dot{\phi}^*_{Rl_2}(r)\phi_{Rl_3}(r) + U^*_{RL_2} \tilde{U}_{RL_3} \phi^*_{Rl_2}(r)\dot{\phi}_{Rl_3}(r) + \tilde{U}^*_{RL_2} \tilde{U}_{RL_3} \dot{\phi}^*_{Rl_2}(r)\dot{\phi}_{Rl_3}(r)]. \tag{A2}$$

Here we omit the orbital index j for simplicity. The $\theta_R(\mathbf{r})$ is a step function that is unity inside the atomic sphere R, $C_{LL_1L_2}$ is the Gaunt coefficient

$$C_{LL_1L_2} = \int d\Omega Y_L Y^*_{L_1} Y_{L_2} , \tag{A3}$$

and $\tilde{U}$ is

$$\tilde{U}_{RL} = \sum_{R_1,L_1} h_{RLR_1L_1} U_{R_1L_1}. \tag{A4}$$

The SIC energy Eq. (2.7) and potential Eq. (2.9) must be evaluated for this orbital charge density. We separate the contribution into the static Coulomb part and the XC part as

$$V_{\rm SIC}(\mathbf{r}) = -V_H(\mathbf{r}) - V_{\rm XC}(\mathbf{r}), \tag{A5}$$

$$E_{\rm SIC}[n] = -E_H[n] - E_{\rm XC}^{\rm LSDA}[n,0]. \tag{A6}$$

The contribution from the XC is a local function of charge density. We calculated them directly on mesh points in atomic spheres. The resulting potentials are numerically expanded to linear combinations of spherical harmonics in each atomic sphere. As regards the contribution from static Coulomb energy, we get the expressions

$$E_H[n] = \frac{1}{2}\left[\sum_{R,L}\int_0^R dr r^2 n_{RL}(r) V_{RL}^{H-O}(r) - \frac{1}{2w}\sum_{R,L,R_2,L_2} Q_{RL} S_{RL,R_2L_2} Q_{R_2L_2}\right], \tag{A7}$$

$$V_H(\mathbf{r}) = \sum_{R,L}\theta_R(\mathbf{r})\sqrt{4\pi}Y_L(\hat{r}_R) \times \left[V_{RL}^{H-O}(r_R) + V_{RL}^{H-N}(r_R)\right], \tag{A8}$$

$$V_{RL}^{H-O}(r) = \frac{1}{2l+1}\left[\frac{1}{r^{l+1}}\int_0^r dr_2 r_2^{l+2} n_{RL}(r_2) + r^l\int_0^r dr_2 r_2 r^{1-l} n_{RL}(r_2)\right], \tag{A9}$$

$$V_{RL}^{H-N}(r) = -\frac{r^l}{2(2l+1)w^{l+1}}\sum_{R_2\neq R,L_2} S_{RL,R_2L_2} Q_{R_2L_2}, \tag{A10}$$

$$Q_{RL} = \frac{1}{(2l+1)w^l}\int_0^{S_R} dr r^{l+2} n_{RL}(r). \tag{A11}$$

Here w is the average atomic sphere radius and S_{RL,R_2L_2} is the unscreened structure constant.[25] From these equations, the SIC potential is expressed as

$$V_{\rm SIC}(\mathbf{r}) = \sum_{R,L}\theta_R(\mathbf{r})\sqrt{4\pi}Y_L(\hat{r}_R)V_{RL}^{\rm SIC}(r_R). \tag{A12}$$

The V_{RL} in Eq. (2.21) is calculated as

$$V_{RL}^{\mathbf{k}} = V^{\mathbf{k}}(\phi,\phi,rL) + V^{\mathbf{k}}(\phi,\dot{\phi},rL) + \sum_{r',L'} h_{rL,r'L'}^{\mathbf{k}}\left[V^{\mathbf{k}}(\dot{\phi},\phi,r'L') + V^{\mathbf{k}}(\dot{\phi},\dot{\phi},r'L')\right]. \tag{A13}$$

Here

$$V^{\mathbf{k}}(\phi,\phi,rL) = \sum_{\mathbf{T},L'} e^{-i\mathbf{k}\cdot\mathbf{T}}\langle\phi_{(r,\mathbf{T}),L}|V_{\rm SIC}|\phi_{(r,\mathbf{T}),L'}\rangle \times U_{(r,\mathbf{T}),L'}, \tag{A14}$$

$$V^{\mathbf{k}}(\phi,\dot{\phi},rL) = \sum_{\mathbf{T},L'} e^{-i\mathbf{k}\cdot\mathbf{T}}\langle\phi_{(r,\mathbf{T}),L}|V_{\rm SIC}|\dot{\phi}_{(r,\mathbf{T}),L'}\rangle \times \tilde{U}_{(r,\mathbf{T}),L'}, \tag{A15}$$

$$V^{\mathbf{k}}(\dot{\phi},\phi,rL) = \sum_{\mathbf{T},L'} e^{-i\mathbf{k}\cdot\mathbf{T}}\langle\dot{\phi}_{(r,\mathbf{T}),L}|V_{\rm SIC}|\phi_{(r,\mathbf{T}),L'}\rangle \times U_{(r,\mathbf{T}),L'}, \tag{A16}$$

$$V^{\mathbf{k}}(\dot{\phi},\dot{\phi},rL) = \sum_{\mathbf{T},L'} e^{-i\mathbf{k}\cdot\mathbf{T}}\langle\dot{\phi}_{(r,\mathbf{T}),L}|V_{\rm SIC}|\dot{\phi}_{(r,\mathbf{T}),L'}\rangle \times \tilde{U}_{(r,\mathbf{T}),L'}. \tag{A17}$$

The $\langle\phi_{(r,\mathbf{T}),L}|V_{\rm SIC}|\phi_{(r,\mathbf{T}),L'}\rangle$ and similar quantities can be calculated by the radial integration in the atomic sphere $(r,\mathbf{T})$ as

$$\langle\phi_{(r,\mathbf{T}),L}|V_{\rm SIC}|\phi_{(r,\mathbf{T}),L_1}\rangle = \sum_{L_2}\sqrt{4\pi}C_{L_1LL_2} \times \int_0^{S_r} dr r^2\phi_{rl}(r)V_{(r,\mathbf{T})L_2}^{\rm SIC}(r)\phi_{rl_1}(r). \tag{A18}$$

The evaluation of the SIC can be performed independently for each orbital. Thus the required computational time scales linearly with the number of occupied orbitals and the required memory does not depend on it.

[1] P. Hohenberg and W. Kohn, Phys. Rev. **136**, B864 (1964).
[2] W. Kohn and L. J. Sham, Phys. Rev. **140**, A1133 (1965).
[3] R. O. Jones and O. Gunnarsson, Rev. Mod. Phys. **61**, 689 (1989).
[4] U. von Barth and L. Hedin, J. Phys. C **5**, 2064 (1972).
[5] S. H. Vosko, L. Wilk, and M. Nusair, Can. J. Phys. **58**, 1200 (1980).
[6] A. Fujimori and F. Minami, Phys. Rev. B **30**, 957 (1984).
[7] A. Fujimori, N. Kimizuka, T. Akahane, T. Chiba, S. Kimura, F. Minami, K. Siratori, M. Taniguchi, S. Ogawa, and S. Suga, Phys. Rev. B **42**, 7580 (1990).
[8] A. E. Bocquet, T. Mizokawa, T. Saitoh, H. Namatame, and A. Fujimori, Phys. Rev. B **46**, 3771 (1992); **42**, 7580 (1990).
[9] J. van Elp, H. Eskes, P. Kuiper, and G. A. Sawatzky, Phys. Rev. B **45**, 1612 (1992).
[10] J. van Elp, R. H. Potze, H. Eskes, R. Berger, and G. A. Sawatzky, Phys. Rev. B **44**, 1530 (1991).
[11] K. Terakura, T. Oguchi, A. R. Williams, and J. Kübler, Phys. Rev. B **30**, 4734 (1984).
[12] J. P. Perdew and A. Zunger, Phys. Rev. B **23**, 5048 (1981).
[13] R. A. Heaton, J. G. Harrison, and C. C. Lin, Phys. Rev. B **28**, 5992 (1983).
[14] N. Hamada and S. Ohnishi, Phys. Rev. B **34**, 9042 (1986).
[15] Y. Hatsugai and T. Fujiwara, Phys. Rev. B **37**, 1280 (1988).
[16] A. Svane and O. Gunnarsson, Phys. Rev. Lett. **65**, 1148 (1990).
[17] Z. Szotek, W. M. Temmerman, and H. Winter, Phys. Rev. B **47**, 4029 (1993).
[18] N. F. Mott, Proc. R. Soc. London Ser. A **62**, 416 (1949).

[19] M. R. Pederson, R. A. Heaton, and C. C. Lin, J. Chem. Phys. **82**, 2688 (1984).
[20] J. P. Perdew and M. R. Norman, Phys. Rev. B **26**, 545 (1982).
[21] M. Arai and T. Fujiwara, in *Computer Aided Innovation of New Materials II* (North-Holland, Tokyo, 1992).
[22] A. Svane and O. Gunnarsson, Phys. Rev. B **37**, 9917 (1988).
[23] Y. Ishii and K. Terakura, Phys. Rev. B **42**, 10 924 (1990).
[24] J. A. Majewski and P. Vogl, Phys. Rev. B **46**, 12 219 (1992).
[25] O. K. Andersen, O. Jepsen, and K. Glötzel, in *Highlights in Condensed Matter Theory*, edited by F. Basani, F. Fumi, and M. P. Toshi (North-Holland, Amsterdam, 1985).
[26] M. Arai and T. Fujiwara (unpublished).
[27] R. W. Godby, M. Schlüter, and J. Sham, Phys. Rev. B **37**, 10 159 (1988).
[28] M. S. Hybersten and S. G. Louie, Phys. Rev. B **34**, 5390 (1986).
[29] F. Aryastetiawan, Phys. Rev. B **46**, 13 051 (1992).
[30] L.F. Mattheiss, Phys. Rev B **5**, 290 (1972).